Int. J. Electrochem. Sci., 11 **(2016)** 7540 – 7552, doi: 10.20964/2016.09.58

International Journal of ELECTROCHEMICAL SCIENCE
www.electrochemsci.org

Electrogeneration of Diiodoaurate in Dimethylsulfoxide on Gold Substrate and Localized Patterning

Ahmed Kandory[1,2], *Reda Yahiaoui*[3], *Etienne Herth*[3], *Hélène Cattey*[4], *Tijani Gharbi*[1], *Guillaume Herlem*[1,*]

[1] Nanomedicine Lab EA4662, Bat E, Université de Franche-Comté, UFR Sciences & Techniques, 16 route de Gray, 25030 Besançon Cedex, France
[2] Department of Chemistry, College of Science, University of Diyala, Iraq.
[3] Institut FEMTO-ST, UMR CNRS 6174, Department MN2S, 26, chemin de l'épitaphe, 25030 Besançon cedex, France
[4] Institut ICMUB - CNRS 6302, Université de Bourgogne, UFR Sciences et Techniques Mirande, 9 Avenue Alain Savary, 21000 Dijon, France
[*]E-mail: guillaume.herlem@univ-fcomte.fr

Received: 4 January 2016 / *Accepted:* 18 July 2016 / *Published:* 7 August 2016

A localized etching of gold surface by scanning electrochemical microscope technique is presented where a dimethylsulfoxide-based electrolyte charged with iodine is used. The electrogenerated triiodide ion at the platinum ultramicroelectrode tip (feedback mode) acts as an oxidant for gold surface. The effects of electrode diameter and the bias time have been investigated. The approach curve method was used to hold the electrode tip close to the gold surface. A scanning electron microscope is used to observe the etched gold surfaces where disk-shaped dots are generated. The diameter of these holes depends directly on the Pt electrode diameter and the bias time.

Keywords: gold etching; iodine-iodide; DFT; SECM; EQCM; utramicroelectrode

1. INTRODUCTION

Modification of surfaces refers to microstructures fabricated on conducting, semiconducting or insulating substrates by deposition of metallic or nonmetallic materials or etching of the substrate surface. For a long time, different methods have been used for modification of surfaces. The plasma modification technique is extensively used for surface functionalization (grafting of various chemical groups) and its etching by means of strong collision [1-4]. Modification can be also performed through

various other methods such as electron-beam lithography [1], photolithography [2-5], inkjet printing [6], and Langmuir-Blodgett technique [7].

For decades, the patterning approach has been based on the photolithography process consists in transferring the pattern onto a substrate via a mask by optical exposure. The fast progress of surface modification microtechnologies confirms that it is a significant area of research. Indeed, microstructure fabrication has a wide range of technological applications in many different fields including electronic devices [8-11], sensors [12, 13], catalysts and data storage [14].

Amongst probing techniques, the scanning electrochemical microscope (SECM) has attracted more attention from researchers due to the coupling of electrochemistry and near-field microscopy since its development mainly in 1989 by A. Bard and co-workers [15]. SECM has been used for localized modification of surfaces through their operating modes: (i) feedback [16] and (ii) direct mode [17]. The higher resolution which is obtained by using the SECM technique made it promising as a powerful tool to study and investigate conducting or insulating surfaces [18, 19].

While photolithography is still the dominant technique for generation of microstructures, intensive efforts have been undertaken in this field. SECM can be considered for the moment as a promising alternative method which is inexpensive for wet etching or biomolecule immobilization [20]. Taking advantage of its etching selectivity [21], mild patterning condition, short period [22], various operating modes [23], and no need to use acids or other corrosive chemicals which used in conventional techniques, SECM technique is more appropriate for surface patterning than others especially since it does not need to preform stamp or mask prior to patterning the substrate.

The feedback mode has been used for localized electrodissolution of high resolution of substrates such as copper [16], GaAs [21, 24], and Si [25, 26]. The process is carried out through locally generated oxidant specie that diffuses toward a substrate surface and reacts therein, producing a localized pattern. The presence of an electroactive redox specie (mediator) in the electrolyte generates at the microelectrode (tip) the desired reaction on the substrate when they are close to one another.

The industrial importance of gold surface, its patterning and applications in the microtechnology industry have been expanded considerably as a result of its unique qualities such as super electrical, thermal and optical conductivities and excellent corrosion resistance behavior. For instance, microlenses can be achieved with gold microholes and are based on gold plasmonic capabilities [27]. Micro-holes in gold foils provide a useful micro-process for manufacturing a flat plane wire winding [28].

The gold pattering step to form functional microstructures is considered as a key to progress of microelectronic fabrication technology. Thus, as previously mentioned, the fabrication technology of bioelectronic devices is mainly dependent on the etching step of material substrates like gold. In fact, it is considered as the most crucial step for increasing the surface area of biosensor platform and in turn for increasing the immobilized biorecognition sensing element [29]. The limit of SECM patterning / etching is the resolution which depends on the probe diameter but also the accuracy of current measurement and positioning system, the probe-to-sample distance, and the Random-walk of ionic diffusion.

A mixture of concentrated hydrochloric acid and nitric acid (aqua regia) has long been the most used etchant for gold [30]. For a long time, cyanides have been used as overwhelming chelating

ligands for electrochemical etching of gold in spite of their toxicity [31]. Over the past decades, intense efforts have been made to develop and find new lixiviants for gold etching. Chen et al. suggested the use of thiourea as a strong complex with gold [32]. Thiosulfate is another gold etchant which has been used in alkaline media [33]. Gold exhibits the ability to form both Au(I) and Au(III) complexes with halides. The stability of the gold complexes depends on the condition of electrolyte but the stability of gold-iodide complexes is greater than the others [34, 35]. KI and Br_2 mixtures are used in clean rooms for wet chemical etching to remove or etch away gold layer [36].

Currently, the iodine-iodide system is well-established for gold patterning as the etchant specie and dates back to the 70s [37]. In this system, the triiodide ion (I_3^-) is generated by the readily reaction of I_2 with I^- ion. The iodide-iodine system has been suggested in several studies for gold etching due to its low oxidizing potential and high solution stability compared to other systems [38]. The iodine/triiodide redox couple in aqueous electrolytes as a mediator and was used in SECM investigation for detecting MnS dissolution products only, not for etching [39].

In the present work, we revisit the use of the iodine-triiodide redox couple but in DMSO and apply it to the localized wet etching of gold surface based on the feedback mode of the SECM technique, where iodine acts as the etchant lixiviate in an aprotic solvent. This new route is based on the formation of reactive oxidizing species able to dissolve gold metal quickly at the micrometer scale. This approach compared to dry etching can achieve improvements such as etch rate in the range 0.1 – 1 µm/min (0.01 – 0.1 µm/min for dry etching), low equipment cost, high chemical and low energy usages.

2. EXPERIMENTAL

2.1. Reagents

The gold substrates used for etching are gold coated (125 nm gold thickness) silicon wafers. Before use, they were rinsed in acetone and ethanol to remove organic contaminants. Absolute ethanol, potassium chloride 99%, acetone 99%, ferrocenemethanol 97% (FcMeOH), dimethylsulfoxide 99% (DMSO), tetrabutylammonium tetrafluoroborate 99% (TBA-BF_4) and iodine 99% were purchased from Aldrich (Saint-Quentin Fallavier, France) and used as received without further purification. The aqueous solutions were prepared by using ultra-pure water obtained in the laboratory (Milli-Q grade).

2.2. Electrochemical Experiments and Procedures

The electrochemical measurements were carried out using a computer-controlled ElProScan PG 340 electrochemical Probe Scanner (HEKA Elektronik, Germany). A positioning system which contains three stepper motors and a piezo translator mounted on a granite portal was used to move the ultramicroelectrode horizontally and vertically close to the surface of the sample. All experiments were carried out at ambient temperature (25°C) in a Faraday cage to minimize background noise, and on an optical table to avoid mechanical vibration.

A three-electrode setup was used for the electrochemical measurements. Home-made disk-shaped platinum ultramicroelectrodes (UMEs) of 5 and 10 µm diameter and microelectrode of 76 µm diameter were used as working electrodes. The UMEs consisted of sealed platinum wires in the fused glass of Pasteur pipette by blowpipe and polished with diamond paste. Platinum wire was used as counter electrode and Ag wire used as a silver reference electrode (SRE).

The microdisk electrodes were characterized electrochemically by studying the steady-state voltammetry of ferrocenemethanol 5 mM in an aqueous solution charged with KCl 0.1 M at low scan rate (20 mV/s). The working electrode (Pt UME) was biased at 0.30 V (oxidation potential of the FcMeOH mediator), the approach curve $I_t/I_{t\infty}$ versus normalized tip-substrate separation L, was recorded for positioning the UME just 2 µm above the gold surface. Notice that the tip was approached to the gold surface and allowed to touch it (contact point) until there is a constant current, and then withdrawn 2 µm above the surface. The normalized current of the approach curve using FcMeOH at the tip i(T) as a function of normalized distance L is shown in Figure 1.

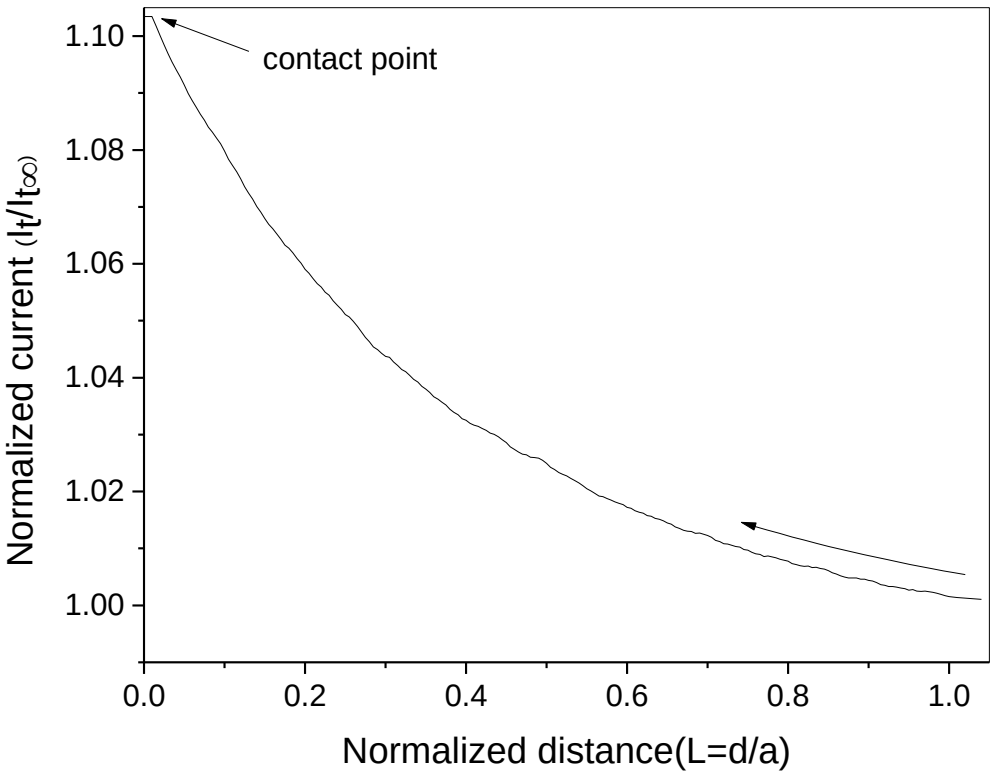

Figure 1. Current-distance curve for 76µm Pt UME biased at 0.30 V vs. SRE approaching a gold surface in aqueous solution containing FcMeOH 5mM plus KCl 0.1 M.

For etching purpose, the electrolyte consists in iodine 5 mM plus TBA-BF_4 0.1 M in DMSO. TBA-BF_4 was used as a supporting electrolyte due to its wide potential stability. The electrochemical behavior of I_2 in DMSO was investigated by cyclic voltammetry on Pt UME for determining the potential to apply at the electrode tip for reducing iodine. The microelectrode potential was then set to the potential value (0.40 V) to electrogenerate triiodide ion at the tip of the UME, and triggering the attack of the gold surface.

DMSO is aprotic and its pKa is about 35 giving it an extremely weak acid behavior. Despite this condition, the iodide-iodine system is stable in this solvent because no precipitate is observed since AuI_2^- complex is known to decompose, leading to gold precipitate [40].

Quartz crystal microbalance (QCM) coupled to cyclic voltammetry was used to monitor mass variation versus potential (PM710, Maxtek, USA) [41]. 5 MHZ polished gold AT-cut quartz crystals (Inficon, USA) were used as working electrode (1.37 cm^2 area). The experiments were performed at room temperature in DMSO-based electrolyte charged with iodine 5 mM plus 0.1 M TBA-BF_4. The electrode potential was repeatedly swept from 0.70 to 0.0 V at a scan rate of 100 mV/s. The correlation between changes of oscillation frequencies of the piezoelectric crystal with the mass deposited on it is based on the Kanazawa – Gordon modelization (the resonant frequency is damped by the viscosity of the liquid) [42].

2.3. UV-Visible spectroscopy

UV-visible absorption spectra were measured by a PerkinElmer UVscan 35 spectrophotometer with one pair of 10-mm quartz cells (115-QS, Hellma).

2.4. 3D surface profilometer

A Tencor Alpha Step IQ profilometer apparatus (Tencor,) was used for measurements.

2.5. Computational Methods

Diiodoaurate linear geometry and triiodide structure which is linear due to iodine lone pairs come from crystallographic data [43-45] All structures were optimized in the presence of the DMSO within the solvent reaction field by using the Polarizable Continuum Model (PCM) at the B3LYP level of theory with the all-electron double zeta plus polarization functions (DZP) basis set [46-48]. Time dependent density functional theory (TD-DFT) calculations were performed on the optimized structures to obtain the excited states (Nstates=20) [49, 50].

3. RESULTS AND DISCUSSION

The study of iodine by cyclic voltammetry in various solvents has been performed by many researchers. Some recent works deal with the mechanism of iodine reduction [51-53]. Nakata et al. have investigated the electrochemical reduction of iodine in a nonaqueous solvent, e.g., acetonitrile (MeCN), dimethylformamide (DMF), DMSO at a mercury and platinum electrode [54]. In the present work, DMSO is used as solvent due to its common properties such as a wide electrochemical window, high electrical conductivity and good thermal and chemical stability [55]. From the hard and soft acids and bases (HSAB) principle, a highly polarizable ion such as iodine is a soft base, and a transition

metal with low charge density such as Au^+ is considered to be soft acid, explaining their propensity to bind [27]. In this context, Figure 2a shows the cyclic voltammogram of iodine in DMSO on Pt microelectrode (76 µm diameter) at a scan rate of 100 mV/s. This is a two-step reduction process with an electron stoichiometry of 1:2 which is observed on Pt electrode.

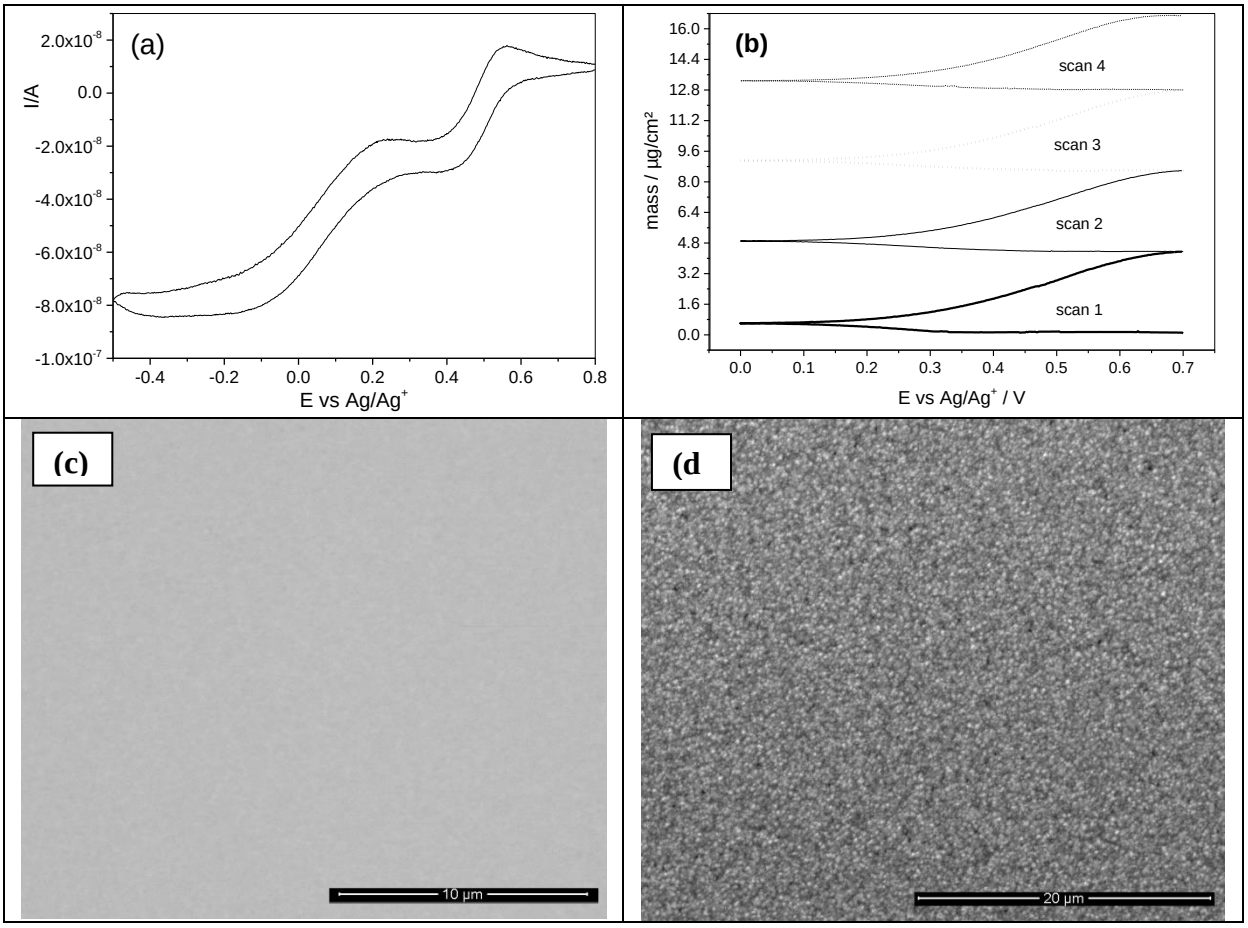

Figure 2. (a) cyclic voltammogram of iodine reduction in DMSO containing TBA-BF_4 0.1 M on Pt UME (76µm) at a scan rate of 100 mV/s and (b) the gold dissolution monitored by EQCM measurement. Gold surface imaged by SEM (c) before reduction below the first wave and (d) after dissolution for 1 min at 0.30 V.

As it is noticeable, the reduction of iodine gives two cathodic waves (wave 1 at 0.40 V and 2 at 0.04 V) which corresponds to the formation of triiodide ion from the reduction of iodine followed by a reduction of triiodide to form iodide as shown in equations (1) and (2) [54].

$$3I_2 + 2e^- \rightleftharpoons 2I_3^- \quad (1)$$

$$2I_3^- + 4e^- \rightleftharpoons 6I^- \quad (2)$$

The triiodide ion which is considered as effective oxidant specie towards gold is electrogenerated at the first cathodic wave, and at the second one triiodide is reduced firstly to iodide. This is followed by a chemical reaction between electrogenerated iodide ion and iodine which is present in the medium as shown eq. 3 below:

$$I_2 + I^- \rightleftharpoons I_3^- \quad (3)$$

The anodic waves refer to reoxidation of iodide and triiodide ions, respectively. Despite the fact that the stability constant of this reaction is highly solvent dependent, the electrochemical behavior on gold in DMSO is similar to that observed in imidazolium-based ionic liquid at room temperature [52].

A cyclic voltammetry investigation (Fig. 2a) coupled to EQCM was carried out to study the dissolution of the gold surface in iodine aprotic solution versus the applied potential. The response was significant for the measurement of electrode mass changes and monitored by EQCM. Figure 2b shows the gold mass loss related to the chemical reaction occurring on the gold surface between the electrode surface material and the generated oxidant species (I_3^-) to form an AuI_2^- complex. The gold dissolution process is not linear over the potential range [0.7 V; 0 V]. Indeed, the dissolution process is quite important between the first reduction wave at 0.40 V and before the second reduction wave at 0.05 V, when triiodide ion is electrogenerated.

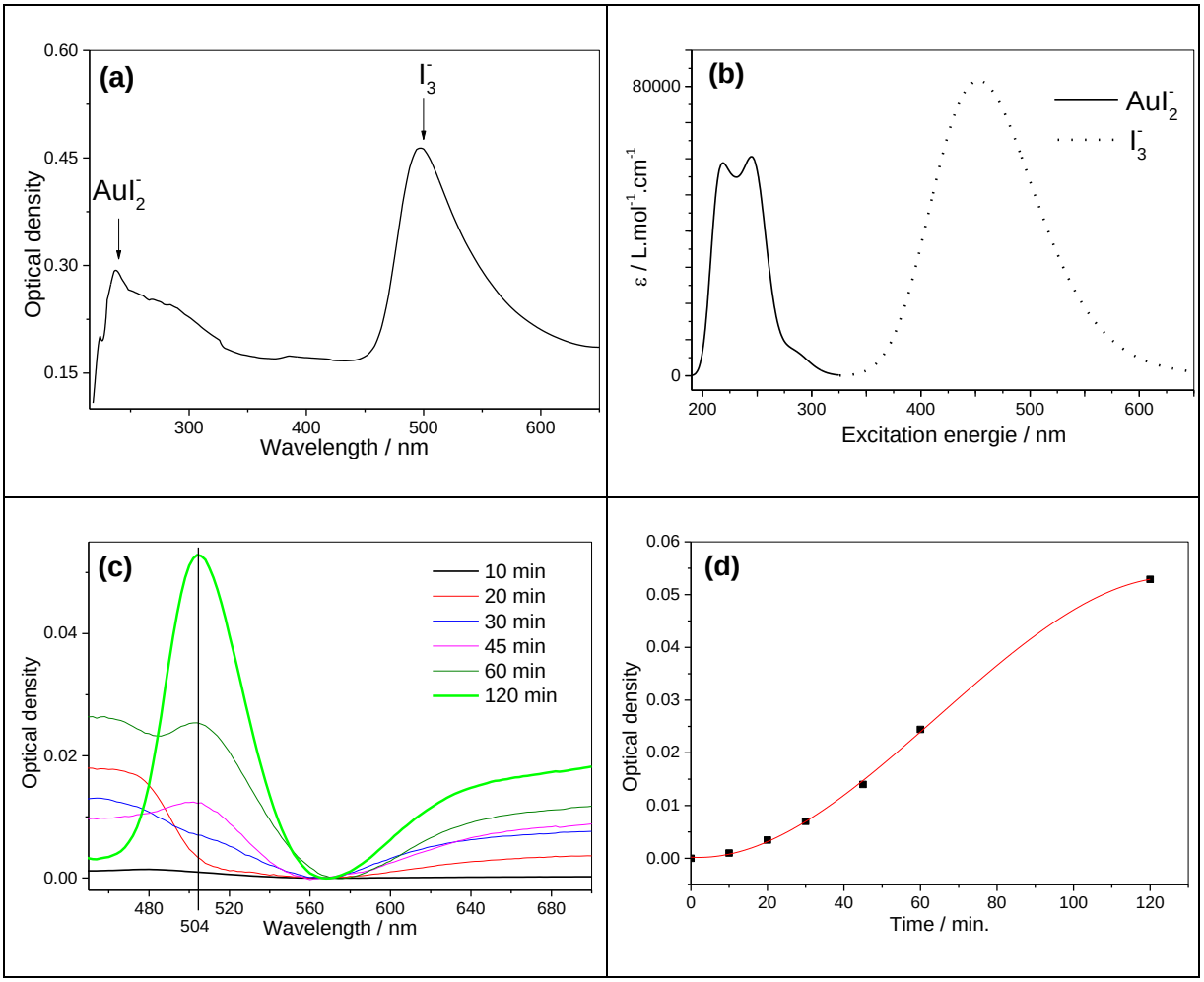

Figure 3. (a) Experimental UV-visible spectrum of TBA-AuI_2 with I_3^- impurity bands in the presence of iodine and (b) theoretical spectra of AuI_2^- and I_3^- solvated in DMSO (PCM model). (c) Absorption curves normalized with optical density value measured at 466 nm (global minimum common to all samples) versus biaising time (at 0.30 V) and (d) data fitting of maximum optical density at 504 nm versus biasing time (at 0.30 V).

Notice that there is no mass loss when cycling in the ranges [1.10 V; 0. 6 V] and [0.00 V; -0. 2 V]. During one scan between 0.70 and 0 V, 16.50 µg/cm² is dissolved in the electrolyte (Figure 2b) and the process is reproducible (as displayed by the four scans) until gold is completely dissolved. The gold electrode surface state was examined by SEM and Figure 2d shows the roughness after biasing at 0.30 V during 1 min compared to the smooth polycrystalline surface (Figure 2c).

During the gold electrodissolution experiment (between the two reduction waves), the electrolyte color changes from deep red-brown to yellow when electrolysis continues for a long time. After biasing at 0.30 V for 120 min, the color of the electrolyte changes and the formation of TBA-AuI_2 and I_3^- in the experimental UV-visible spectrum (Figure 3a) [56]. It means that diiodoaurate anion in DMSO is colorless. Moreover, it absorbs in the ultraviolet region as it is observed for the solid salt TBA-AuI_2 [57]. From quantum chemistry modelization, it is possible to confirm that diiodoaurate anion absorbs only in the UV region while triiodate anion has a band in the visible region as displayed Figure 3b.

The dissolution of gold in this case can be monitored by a colorimetric titration of triiodide ion until the entire iodine quantity is consumed. Indeed, there is an increase of band height at 504 nm during electrolysis (Figure 3a) which can be monitored more easily than that of diiodoaurate anion at 235 nm. The superimposition of normalized absorption curves (at 566 nm because of the global minimum common to all spectra) during electrolysis at 0.30 V versus time is shown in Figure 3c. The optical density values at 504 nm (peak) reported versus time can be fitted by a third order polynomial equation ($R^2 = 0.999$).

The formation process of microstructured holes on the gold substrate via SECM etching was achieved successfully by taking into account the effect of tip diameter, the gap between the tip and the surface and biasing time. Indeed, the resolution of the microstructures generated by this method is controlled by these three parameters. Various experiments were conducted to study the effect of the ultramicroelectrode diameter, the gap between the UME tip and gold surface and the electrolysis duration on the size of microstructure pattern. In this context, the electrode tip biased at a constant potential (0.40 V) for different durations: 30, 60, 90, 120, 150, 180 sec and UMEs having different diameters were used. At 0.40 V, iodine reduction took place as the gold etching solution vicinity to electrode tip contains the two important components for gold etching: I^- and I_3^-. The complexing agent (I^-) forms a stable complex with gold while the oxidant (I_3^-) establishes the potential of the surface at a value where significant gold dissolution can occur. In this working environment, the gold surface patterning took place successfully due to the surface attack by triiodide ion. In the presence of iodide ions, gold is dissolved and forms a very stable complex AuI_2^-:

$$2Au + I^- + I_3^- \rightarrow 2AuI_2^- \qquad (4)$$

Several circular holes were formed in the gold surface by positioning the electrode tip on different sites of the gold surface. These microstructures were characterized by SEM and profilometry as shown in Figure 4.

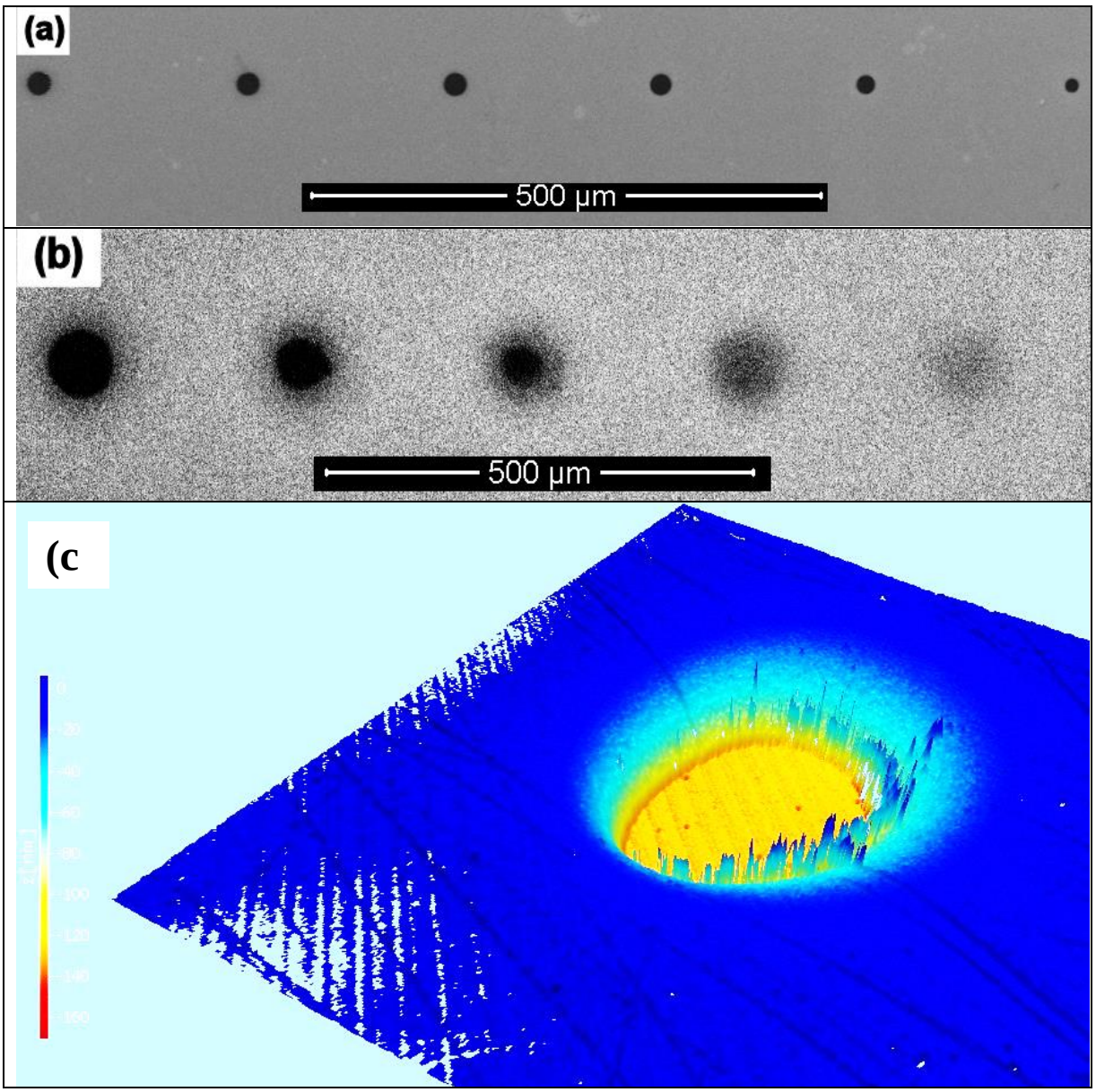

Figure 4. (a) Electronic microscopy of gold etching by SECM. (b) Effect of the gap between the tip and the gold substrate on the hole boundary. (c) 3D surface profilometer image of the hole after gold etching by SECM.

Considering the electrolysis time, it is noted that large diameter patterned-disks were formed by increasing the electrolysis duration due to the diffusion of the oxidant specie (I_3^-) laterally far away from the tip of electrode and along the surface which promotes further etching of the surface more than the tip area. As shown in Figure 4a (from right to left), the diameter of the holes increased with electrolysis time. For instance, a hole with a 12.75 µm diameter is obtained after 30 s bias time while a 22.7 µm diameter dot is obtained after 180 s bias time when a 10 µm diameter Pt ultramicroelectrode is used.

Regarding the effect of the tip-to-sample distance, it was found that the gap distance has a great impact on the dissolution rate and the diameter of the generated dots. As shown in Figure 4b, the

effective distance between 2-4 µm has the fastest etching rate with a well-defined boundary hole while a more important gap (by going to the right in Figure 4b) leads to poorly-defined boundaries. Regarding the size of generated dots, it was found that it is inversely proportional to the gap distance. Discussion for Fig. 4c with flat bottom, well-defined boundaries are achieved with a gap between the tip and the substrate that is 4 µm and reproducibility.

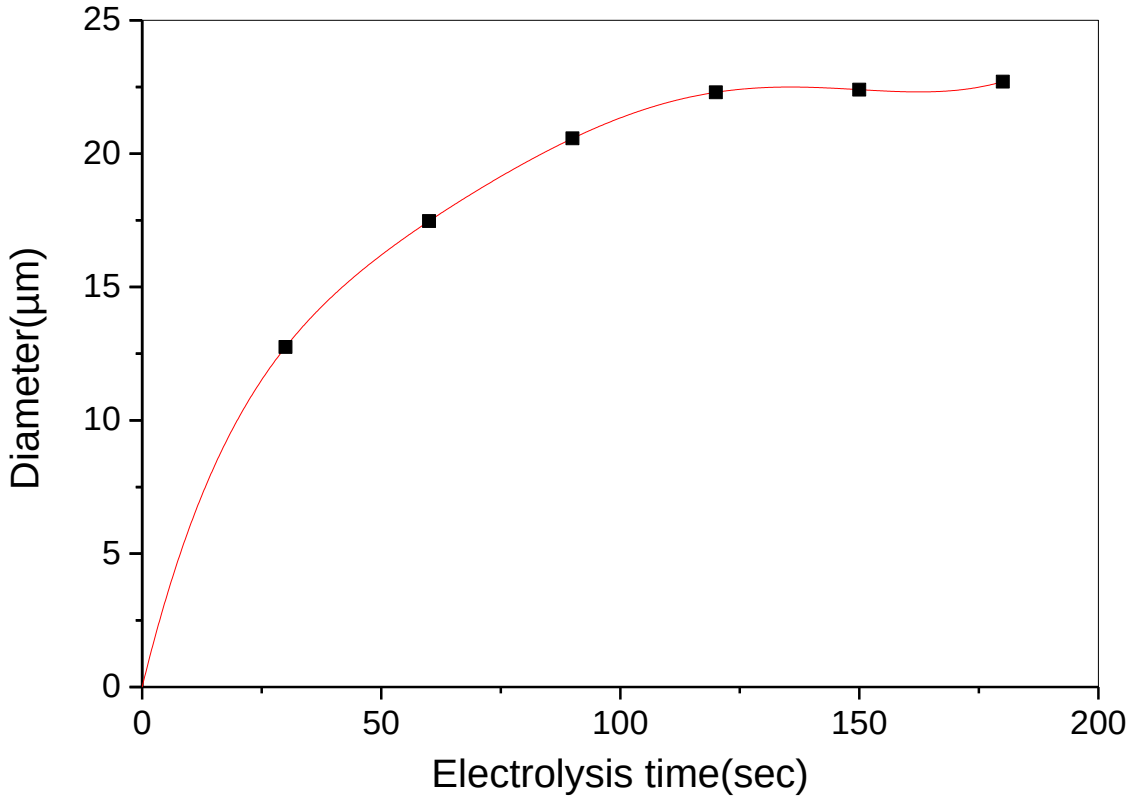

Figure 5. Diameter of circular dots generated on the gold surface as a function of biasing time.

It is well known that the UME diameter acts on the steady-state current value and thus on the etched pattern size. Considering the electrolysis time, it is noted that large diameter-patterned disks were formed by increasing the electrolysis duration due to the diffusion of the oxidant species (I_3^-) far away from the tip of electrode. As shown in Figure 5, the diameter of the holes increases in a hyperbolic way with electrolysis time. Notice that from the extrapolation curve in red (third order polynomial fitting), it is possible to achieve holes with submicrometer size in less than few seconds with the use of a nanoelectrode (nanode) if the gold substrate thickness is 125 nm.

Anyway, the wet etching method which is used in this work is simple and economical [58] compared to dry methods. Indeed, they are not recommended for gold surface etching because of the re-deposition of non-volatile gold complexes [59]. On the contrary of other wet methods, the etching by iodine solution has some advantages such as more cost effective (etching solution contained just one component), one-step procedure, environment friendly method since the leaching by cyanide has a several substantial drawbacks like the high toxicity [35, 60]. Using the thiosulfate as an alternative

complexing ligand for gold etching causes inhabitation by the formation of a passive layer that prevents the full dissolution of gold [61].

On the other hand, using SECM as local maskless etching technique made it a simplest method of surface etching with high control of size and depth of generated grooves. Clean etching process which can be obtained by using SECM, is one of the most important feature to ensure the electrical and optical properties of the remaining film are preserved [62].

4. CONCLUSIONS

In this study, we demonstrated that local etching of a gold surface with iodine in DMSO-based electrolyte can be performed successfully by using wet electrochemical etching. The band of the triiodide anion at 504 nm and electrogenerated on gold in DMSO can be monitored by visible spectroscopy instead of the diiodoaurate one which is more difficult to observe. Microstructure holes were made by using SECM technique through electrogeneration of oxidant specie (I_3^-) at the tip of UME. It was shown that the size of the electrogenerated holes directly depends on the diameter of UME used, gap distance between gold surface and the tip of UME and biasing time. In all cases, the diameter of electrogenerated circular dots is greater than that of the UME used. The reason comes from the diffusion of oxidant species near the electrode tip.

ACKNOWLEDGEMENT
We gratefully acknowledge the Iraqi Ministry of Higher Education and the Scientific Research and Cultural Bureau /Embassy of the Republic of Iraq in Paris – France for financial support. This work was also supported by Campus France and the Region of Franche-Comté. Computations were performed at the supercomputer facilities of the “Mésocentre de calcul de Franche-Comté”, France.

References

1. S. Kishimoto, N. Shinya and M. D. Mathew, *Journal of Materials Science*, 32 (1997) 3411
2. D. Ryan, B. A. Parviz, V. Linder, V. Semetey, S. K. Sia, J. Su, M. Mrksich and G. M. Whitesides, *Langmuir*, 20 (2004) 9080
3. S.-H. Lee, J. J. Moon and J. L. West, *Biomaterials*, 29 (2008) 2962
4. H. Wu, T. W. Odom and G. M. Whitesides, *Analytical Chemistry*, 74 (2002) 3267
5. P. Prompinit, A. S. Achalkumar, X. Han, R. J. Bushby, C. Wälti and S. D. Evans, *The Journal of Physical Chemistry C*, 113 (2009) 21642
6. K. C. Yung, S. P. Wu and H. Liem, *Journal of Materials Science*, 44 (2009) 154
7. Y. Kado, A. Aoki and T. Miyashita, *Journal of Materials Science*, 37 (2002) 4839
8. S. K. Ghandhi, *S. K. Ghandhi, VLSI Fabrication Principles, p.475, John Wiley &Sons, Inc., New York (1983)*, p. 475, New york (1983).
9. B. Tuck, *Journal of Materials Science*, 10 (1975) 321
10. S.-C. Hung, O. A. Nafday, J. R. Haaheim, F. Ren, G. C. Chi and S. J. Pearton, *The Journal of Physical Chemistry C*, 114 (2010) 9672
11. T. Bhuvana and G. U. Kulkarni, *ACS Nano*, 2 (2008) 457
12. L. Rassaei, P. S. Singh and S. G. Lemay, *Analytical Chemistry*, 83 (2011) 3974

13. S. Daniele, E. De Faveri, I. Kleps and A. Angelescu, *Electroanalysis*, 18 (2006) 1749
14. S. Y. Chou, M. S. Wei, P. R. Krauss and P. B. Fischer, *Journal of Applied Physics*, 76 (1994) 6673
15. A. J. Bard, F. R. F. Fan, J. Kwak and O. Lev, *Analytical Chemistry*, 61 (1989) 132
16. D. Mandler and A. J. Bard, *Journal of The Electrochemical Society*, 136 (1989) 3143
17. D. H. Craston, C. W. Lin and A. J. Bard, *Journal of The Electrochemical Society*, 135 (1988) 785
18. G. Wittstock, M. Burchardt, S. E. Pust, Y. Shen and C. Zhao, *Angewandte Chemie International Edition*, 46 (2007) 1584
19. D. Mandler, *Scanning Electrochemical Microscopy*, Marcel-Dekker, New York (2001).
20. J. Shao, E. A. Josephs, C. Lee, A. Lopez and T. Ye, *ACS Nano*, 7 (2013) 5421
21. D. Mandler and A. J. Bard, *Langmuir*, 6 (1990) 1489
22. C.-A. McGeouch, M. Peruffo, M. A. Edwards, L. A. Bindley, R. A. Lazenby, M. M. Mbogoro, K. McKelvey and P. R. Unwin, *The Journal of Physical Chemistry C*, 116 (2012) 14892
23. W. B. Nowall, D. O. Wipf and W. G. Kuhr, *Analytical Chemistry*, 70 (1998) 2601
24. D. Mandler and A. J. Bard, *Journal of The Electrochemical Society*, 137 (1990) 2468
25. S. Meltzer and D. Mandler, *Journal of the Chemical Society, Faraday Transactions*, 91 (1995) 1019
26. Y. Zu, L. Xie, B. Mao and Z. Tian, *Electrochimica Acta*, 43 (1998) 1683
27. S. Saxena, R. P. Chaudhary, A. Singh, S. Awasthi and S. Shukla, *Sci. Rep.*, 4 (2014)
28. C. Zhiling, L. Sheng, S. Tielin, X. Liangcai, Q. June and Q. Yubin, in *Electronic Packaging Technology Proceedings, 2003. ICEPT 2003. Fifth International Conference on*, p. 172 (2003).
29. S. Marx, M. V. Jose, J. D. Andersen and A. J. Russell, *Biosensors and Bioelectronics*, 26 (2011) 2981
30. T. O. P. Atkins , J. Rourke , M. Weller, F. Armstrong , M. Hagerman, *Inorganic chemistry*, W.H. Freeman, New York (2010).
31. P. H. Qi and J. B. Hiskey, *Hydrometallurgy*, 27 (1991) 47
32. C. K. Chen, T. N. Lung and C. C. Wan, *Hydrometallurgy*, 5 (1980) 207
33. Y. Xia, X.-M. Zhao, E. Kim and G. M. Whitesides, *Chemistry of Materials*, 7 (1995) 2332
34. M. Baghalha, *Hydrometallurgy*, 113–114 (2012) 42
35. H.-x. Wang, C.-b. Sun, S.-y. Li, P.-f. Fu, Y.-g. Song, L. Li and W.-q. Xie, *International Journal of Minerals, Metallurgy, and Materials*, 20 (2013) 323
36. K. R. Williams, K. Gupta and M. Wasilik, *Microelectromechanical Systems, Journal of*, 12 (2003) 761
37. Y. Nemirovsky, I. A. Blech and J. Yahalom, *Journal of The Electrochemical Society*, 125 (1978) 1177
38. J. B. H. a. V. P. Atluri, *Miner. Proc. Extract. Metall. Rev*, 4 (1988) 95
39. C. H. Paik, H. S. White and R. C. Alkire, *Journal of The Electrochemical Society*, 147 (2000) 4120
40. A. Davis, T. Tran and D. R. Young, *Hydrometallurgy*, 32 (1993) 143
41. M. R. Deakin and D. A. Buttry, *Analytical Chemistry*, 61 (1989) 1147A
42. K. K. Kanazawa and J. G. Gordon, *Analytical Chemistry*, 57 (1985) 1770
43. S. Friedrichs and P. G. Jones, *Acta Crystallographica Section C*, 55 (1999) 1625
44. A. J. Blake, C. Caltagirone, V. Lippolis, M. Schroder and C. Wilson, *Acta Crystallographica Section E*, 60 (2004) m20
45. A. Vogler and H. Kunkely, *Coordination Chemistry Reviews*, 219–221 (2001) 489
46. G. Scalmani and M. J. Frisch, *The Journal of Chemical Physics*, 132 (2010) 114110
47. C. L. Barros, P. J. P. de Oliveira, F. E. Jorge, A. Canal Neto and M. Campos, *Molecular Physics*, 108 (2010) 1965
48. A. Canal Neto and F. E. Jorge, *Chemical Physics Letters*, 582 (2013) 158
49. G. Scalmani, M. J. Frisch, B. Mennucci, J. Tomasi, R. Cammi and V. Barone, *The Journal of Chemical Physics*, 124 (2006) 094107
50. M. J. Frisch, G. W. Trucks, H. B. Schlegel, G. E. Scuseria, M. A. Robb, J. R. Cheeseman, G.

Scalmani, V. Barone, B. Mennucci, G. A. Petersson, H. Nakatsuji, M. Caricato, X. Li, H. P. Hratchian, A. F. Izmaylov, J. Bloino, G. Zheng, J. L. Sonnenberg, M. Hada, M. Ehara, K. Toyota, R. Fukuda, J. Hasegawa, M. Ishida, T. Nakajima, Y. Honda, O. Kitao, H. Nakai, T. Vreven, J. A. Montgomery Jr., J. E. Peralta, F. Ogliaro, M. J. Bearpark, J. Heyd, E. N. Brothers, K. N. Kudin, V. N. Staroverov, R. Kobayashi, J. Normand, K. Raghavachari, A. P. Rendell, J. C. Burant, S. S. Iyengar, J. Tomasi, M. Cossi, N. Rega, N. J. Millam, M. Klene, J. E. Knox, J. B. Cross, V. Bakken, C. Adamo, J. Jaramillo, R. Gomperts, R. E. Stratmann, O. Yazyev, A. J. Austin, R. Cammi, C. Pomelli, J. W. Ochterski, R. L. Martin, K. Morokuma, V. G. Zakrzewski, G. A. Voth, P. Salvador, J. J. Dannenberg, S. Dapprich, A. D. Daniels, Ö. Farkas, J. B. Foresman, J. V. Ortiz, J. Cioslowski and D. J. Fox, Gaussian 09, in, Gaussian, Inc., Wallingford, CT, USA (2009).
51. E. I. Rogers, I. Streeter, L. Aldous, C. Hardacre and R. G. Compton, *The Journal of Physical Chemistry C*, 112 (2008) 10976
52. C. L. Bentley, A. M. Bond, A. F. Hollenkamp, P. J. Mahon and J. Zhang, *Analytical Chemistry*, 85 (2013) 11319
53. C. L. Bentley, A. M. Bond, A. F. Hollenkamp, P. J. Mahon and J. Zhang, *The Journal of Physical Chemistry C*, 118 (2014) 22439
54. R. Nakata, S. Okazaki and T. Fujinaga, *Journal of Electroanalytical Chemistry and Interfacial Electrochemistry*, 125 (1981) 413
55. W. Le, K. Du, L. Zhang, J. Xiao, C. Zhang, Y. Zhang, L. Zhou and Q. Yin, *Electrochimica Acta*, 95 (2013) 179
56. P. Klæboe, *Acta Chemica Scandinavica*, 18 (1964) 27
57. I. Ohtsuka, H. Nakayama and K. Ishii, *Journal of Raman Spectroscopy*, 20 (1989) 489
58. T.-S. Choi and D. W. Hess, *ECS Journal of Solid State Science and Technology*, 4 (2015) N3084
59. T. Y. Kang, G. Kim, I. H. Cho, D. Seo and S. J. Hong, *Thin Solid Films*, 517 (2009) 3919
60. S. S. Konyratbekova, A. Baikonurova and A. Akcil, *Mineral Processing and Extractive Metallurgy Review*, 36 (2015) 198
61. S. R. Smith, J. J. Leitch, C. Zhou, J. Mirza, S.-B. Li, X.-D. Tian, Y.-F. Huang, Z.-Q. Tian, J. Y. Baron, Y. Choi and J. Lipkowski, *Analytical Chemistry*, 87 (2015) 3791
62. F. Grisotto, R. Metaye, B. Jousselme, B. Geffroy, S. Palacin and J. Charlier, *Journal of Materials Chemistry*, 21 (2011) 15962